



저작자표시-비영리 2.0 대한민국

이용자는 아래의 조건을 따르는 경우에 한하여 자유롭게

- 이 저작물을 복제, 배포, 전송, 전시, 공연 및 방송할 수 있습니다.
- 이차적 저작물을 작성할 수 있습니다.

다음과 같은 조건을 따라야 합니다:



저작자표시. 귀하는 원저작자를 표시하여야 합니다.



비영리. 귀하는 이 저작물을 영리 목적으로 이용할 수 없습니다.

- 귀하는, 이 저작물의 재이용이나 배포의 경우, 이 저작물에 적용된 이용허락조건을 명확하게 나타내어야 합니다.
- 저작권자로부터 별도의 허가를 받으면 이러한 조건들은 적용되지 않습니다.

저작권법에 따른 이용자의 권리는 위의 내용에 의하여 영향을 받지 않습니다.

이것은 [이용허락규약\(Legal Code\)](#)을 이해하기 쉽게 요약한 것입니다.

[Disclaimer](#) 

Thesis for the Degree of Master of Science

Fabrication of Sub-micron $\text{Al}(\text{OH})_3$
Structures Local Enhancing Gold
Photoluminescence by Dip-Pen Lithography
and Polymer Pen Lithography



by

Jehyeok Ryu

Department of physics

The Graduate School

Pukyong National University

February 2020

Fabrication of Sub-micron $\text{Al}(\text{OH})_3$
Structures Local Enhancing Gold
Photoluminescence by Dip-Pen Lithography
and Polymer Pen Lithography

(딥펜리소그래피와 폴리머펜
리소그래피로 만든 알루미늄
수산화물의 금 광발광 향상 효과)

Advisor: Prof. Jae Won Jang

by

Jehyeok Ryu

A thesis submitted in partial fulfillment of the requirements

for the degree of Master of Science

in Department of Physics, The Graduate School,

Pukyong National University

February 2020

Fabrication of Sub-micron Al(OH)₃ Structures Local Enhancing Gold
Photoluminescence by Dip-Pen Lithography and Polymer Pen
Lithography

A dissertation

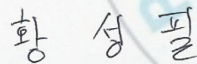
by

Jehyeok Ryu

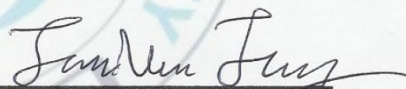
Approved by



(Chairman) Heeso Noh



(Member) Seongpil Hwang



(Member) Jae-Won Jang

February 2020

Table of Contents

Abstract	iv
1. Introduction	1
2. Experimental Section	4
2.1. Fabrication of sub-micron Al(OH) ₃ structures	4
2.2. Structural analysis with atomic force microscopy and kelvin probe force microscopy	5
2.3. Elemental analysis with electron probe micro-analyzer and time-of-flight secondary ion mass spectrometry	5
2.4. Photoluminescence measurement	6
3. Results and Discussion	7
4. Conclusion	37
5. References	38

Figure List

Figure 1. Schematic illustrations of the dip-pen nanolithography (DPN) process	2
Figure 2. Optical microscopy and scanning electron microscopy (SEM) image of the DPN processed structure with liquid phase transfer method	3
Figure 3. Atomic force microscopy (AFM) and kelvin probe force microscopy (KPFM) analysis of the DPN processed structure with liquid phase transfer method	4
Figure 4. Electron probe micro-analysis (EPMA) on the DPN processed structure with liquid phase transfer method	5
Figure 5. AFM, KPFM and Time of Flight Secondary Ion Mass Spectroscopy (TOF-SIMS) analysis on the DPN processed structure with solid-gel phase transfer method	6
Figure 6. AFM and phase image of the DPN processed $\text{Al}(\text{OH})_3$ structure with solid-gel phase transfer method and liquid phase transfer method	7
Figure 7. AFM analysis of the DPN processed line structure	8
Figure 8. Optical microscopy and AFM image of the polymer pen lithography (PPL) processed $\text{Al}(\text{OH})_3$ structures with liquid phase transfer method and solid-gel phase transfer method	9
Figure 9. Fluorescence image of the PPL processed structure with liquid phase transfer method and solid-gel phase transfer method	11

Figure 10. Micro photoluminescence of the PPL processed structure with solid-gel phase transfer method 12

Figure 11. Fluorescence image and macro photoluminescence spectrum of the macro hole Al(OH)₃ structure 13

Figure 12. Optical microscopy and fluorescence image of the isolated Al(OH)₃ structure..... 14



딥펜리소그래피와 폴리머 펜 리소그래피로 만든 알루미늄 수산화물의 금 광발광 향상 효과

류제혁

부경대학교 대학원 물리학과

요약

딥펜리소그래피와 폴리머 펜 리소그래피를 이용한 알루미늄 수산화물을 마이크로, 나노영역에서 제작하였다. 두 리소그래피를 이용한 공정에서, 고체-겔 상 전사방법과 액체 상 전사방법을 통해 수산화이온을 금 20 나노미터, 알루미늄 100 나노미터, 실리콘 기판 위에 국소적으로 전사하였다. 이 국소적인 전사를 통하여, 수산화이온은 금 밑의 알루미늄 층과 화학반응을 일으킬 수 있었고 그에 따라 마이크로미터, 나노미터 크기의 솟아오른 알루미늄 수산화물이 형성되었다. 액체 상 전사방법을 통하여 얻은 솟아오른 알루미늄 수산화물은 지름이 6 마이크로미터 이상에서만 구현되는 반면에, 고체-겔 상 전사방법을 이용하면 지름 1 마이크로미터 이하 영역의 구조물을 얻을 수 있었다. 형성된 물질의 구조와 형성과정이 켈빈 탐침력 현미경을 이용하여 분석되었고, 형성과정 중 금 막 밑의 알루미늄이 반응된 것을 확인하였다. 원소분석방법으로서, 전자탐침 미세 분석기와 비행시간형 이차이온질량분석을 통해 구조물이 알루미늄 산화물인 것이 확인되었다. 이외에, 기판 위의 알루미늄 수산화물 패턴들에서 파란 빛 영역대의 형광이미지가 관측되었고 광발광 스펙트럼을 통해 알루미늄 수산화물이 금 기판의 광발광 효율을 향상시키는 것을 확인하였다.

Introduction

It has been tremendous demands for lithography to fabricate sub-micron/microstructures to obtain exceptional optical characteristics since such low scaled materials manifest dominant surface properties due to its high surface/volume ratio. In order to meet the need for the low scaled fabrication, two approaches as top-down and bottom-up have been employed. First of all, the top-down approach is a lithographic way to fabricate nanostructures from bulk states of structures, e.g., photolithography, e-beam lithography. The photolithography can produce large patterned area and require relatively short operation time, however, it has lower limitation for a dimension of length in a structure due to its wavelength-dependence on the light employed in the lithographic process. The e-beam lithography, on the other hand, has an advantage to high resolution in the fabrication but requires considerable costs and time with a limited engineered area. Secondly, the bottom-up approach is a lithographic way to transfer target materials to a substrate such as nano-imprint, self-assembly monolayer method, soft lithography. The lithographies based on bottom-up approach have benefits with a low-cost, facile operating process, but lack of controllability to geometries, and low resolution.

Therefore, tip-based nanolithography (TBN) can be a proper candidate for low scaled fabrication. TBN is a lithographic tool which employs nano-scaled tip to fabricate local structures on a substrate based on scanning tunneling microscopy (STM), atomic force microscopy (AFM) and polymer pen lithography (PPL).¹ Among these TBN approaches, nano-scaled materials could be engineered through various mechanisms for the fabrication; e.g, atom-removing²⁻³, thermal⁴, electro-

chemical⁵⁻⁶, optical⁷⁻⁸, molecular diffusion⁹⁻¹², mechanical removal¹³, and field emission¹⁴ due to the availability to tune physical properties on the tip. In particular, the electrochemical using the TBN can trigger local oxidation on a metal substrate that has significant potential to investigate characteristics of nanometal oxide. For example, the local oxidation process can be conducted using STM, which apply electric current between the tip and the substrate.¹⁵ However, it is necessary to maintain a low-temperature ultra-high vacuum environment for the tunneling effect which is a principle of STM. Dip-pen nanolithography (DPN) is derived from the AFM platform as a lithographic tool. As opposed to the STM, it is attainable to conduct in an ambient atmosphere and room temperature, which makes it straightforward to utilize. Moreover, applying an electric bias between an AFM tip and a substrate yields the meniscus to dissociate with H⁺ and OH⁻ ions, followed by the local oxidation process.^{5, 16-17} Despite the potential of fabrication approaches applying various methods mentioned above, the DPN still struggle to produce a large-area patterned sample. It is reported that elastomeric tip arrays with about 11 million pyramid-shaped pens consisting of polydimethylsiloxane (PDMS) can be used to transfer ink to a substrate in a large-area scale as an alternative of the DPN.¹⁸ Since the polymer pen is elastomeric PDMS tip, contrary to typical hard silicon-based tip, it takes very low costs to make and into no consideration to be damaged.

Here, we employed two ink-transfer methods; solid-gel phase transfer method and liquid phase transfer method, which are similar methods to well known conventional transfer methods (solid transfer, liquid transfer, respectively) in the DPN and PPL,¹⁹⁻²¹ to conduct a local chemical reaction without introducing electric bias between a tip and a substrate. Instead, we inked the tip with 1 M KOH ink as

a source of OH^- ion supply to expose the substrate directly with OH^- ions. To be specific, we named solid-gel phase transfer rather than using solid transfer because the KOH ink would be a mixture of solid and gel phase. Since the KOH ink has super hydrophilic characteristics, a perfect solid phase of KOH ink is barely obtained despite fully drying process. After we obtained protruded $\text{Al}(\text{OH})_3$ structures using two transfer ways, we investigated the photoluminescence properties in our obtained structures.



2. Experimental

2.1. Fabrication of Sub-micron Al(OH)₃ Structures

Conventional thermal evaporation methods were utilized to prepare thin metal film deposited substrate. A 100 nm-thick Al layer as a target layer was deposited on a silicon substrate. Then, a 20 nm-thick Au layer was sequentially deposited on the substrate. Evaporation steps were conducted at a $\sim 0.1 \text{ \AA/s}$ deposition rate for both Au and Al layer.

For the fabrication of Al(OH)₃ structures with solid-gel phase transfer, a SiN tip cantilever (M-type, NanoInk Inc., USA) was immersed in 2 mL of 1 M KOH ink for 2 min. Then, the KOH-inked SiN tip cantilever was fully dried for 1 h in the ambient atmosphere. The prepared tip cantilever was adjusted to the commercially available nanolithography platform (DPN5000, NanoInk Inc., USA) and engaged to the surface of the substrate. The tip dwelled consistently on the surface for 10 min forming Al(OH)₃ structures in a chamber to maintain humidity to 50%. The DPN processed sample was sequentially rinsed with DI water and dried by N₂ gas. For large-area patterned Al(OH)₃ structures by solid-gel phase transfer, polymer pen was prepared following the same step of the DPN process. To engage polymer pen to the substrate, an AFM equipment for lithography (TT-2 AFM, AFMWorkshop, USA) was utilized in a chamber with 30% humidity.

For the fabrication of Al(OH)₃ structures with liquid phase transfer, both the KOH inked SiN tip cantilever and polymer pen were employed without the drying process. The KOH inked SiN tip and polymer pen adjusted to the DPN5000 and

TT-2 AFM, respectively, were engaged to the substrate and withdrawn after it dwelled on the substrate for 1 s.

2.2. Structural Analysis with Atomic Force Microscopy and Kelvin Probe Force Microscopy

Topography, phase images and electric potential mapping were obtained using amplitude-modulated kelvin probe force microscopy (KPFM) mode in an atomic force microscopy instrument (Dimension Icon, Bruker Co., USA) using a Pt/Ir-coated tip (SCM-PIT, Bruker Co., USA).

2.3. Elemental Analysis with Electron Probe Micro-Analysis and Time-of-Flight Secondary Ion Mass Spectrometry.

For elemental characterization of DPN processed structures, composition analysis was studied using electron probe micro-analysis (EPMA) of JXA-8530F (JEOL Ltd.) accelerated by the voltage at 15 kV and probed by the current at 60 nA. Al, O, Au, and K were selected as elements for EPMA mapping.

Time-of-flight secondary ion mass spectrometry (TOF-SIMS 5, ION-TOF GmbH) was conducted by using a pulsed 30 keV Bi⁺ primary beam with a current 0.55 pA for 500 s data acquisition time. Positive ion spectra were internally calibrated using H⁺, CH₃⁺, C₂H₅⁺, C₃H₇⁺, C₄H₉⁺ normalized to the respective secondary total ion yields. The chemical images of the analyzed area were recorded

with 512×512 pixels resolution during the data acquisition. The depth profile was obtained for 7600 s while etching the analyzed area of $500 \mu\text{m} \times 500 \mu\text{m}$ with Cs beam accelerated at 250 eV.

2.4. Photoluminescence Measurement.

Fluorescence images of the structures on the substrate processed by PPL and soft lithography with a PDMS stamp were obtained using Axio Scope. A1 (Carl Zeiss, Germany). For fluorescent images excited by different wavelength light source with different emission peak, the light source from He lamp was filtered by three fluorescent filters; DAPI (λ_{ext} : 365 nm, λ_{em} : 445 nm), GFP (λ_{ext} : 475nm, λ_{em} : 530 nm), CYAN 5 (λ_{ext} : 545 nm, λ_{em} : 605 nm).

The photoluminescence spectrum of the PPL processed dot structure was measured using LabRam HR800 UV PL microscope (Horiba Jobin-Yvon Inc., Japan). The measurement was conducted using the He-Cd laser with 325 nm wavelength as an excitation source at room temperature. The $2 \mu\text{m}$ diameter excitation laser was irradiated on the dot structure and the substrate for 30 s with accumulation 3 times with power intensity of 10 mW. For the macro photoluminescence measurement, 2 cm diameter excitation source with wavelength 266 nm diode-pumped solid-state laser (DPSS) and 325 nm He-Cd laser were used with power intensity 30 mW and 20 mW, respectively. The excitation lasers were irradiated on the substrate with or without the macro hole patterned structure for 0.1 s with accumulation 50 times.

Result and Discussion

In our previous study, we fabricated macro $\text{Al}(\text{OH})_3$ hole structure on a substrate using Au nanomembrane-based micro/nanolithography.²² As an Au layer was deposited on prepared Al/ Si substrate by thermal evaporation, it includes few nanometer pores till the thickness of the evaporated Au membrane reached 40 nm. Hence, the Au layer controls the volume of ion to be transported to the indicating layer relatively uniform rate, resulting in the fine construction of the obtained structures.²³ In the lithography, the reacted Al layer showed two-tone structures depending on the volume of KOH ink used in the fabrication process. The protruded $\text{Al}(\text{OH})_3$ structures were engineered on the Au membrane when the relatively smaller volume of KOH ink was used, while the recessed tunnel structures under the Au membrane were present due to the etching process of the Al layer from a relatively larger volume of KOH ink.

Here, to investigate the process of the protruded $\text{Al}(\text{OH})_3$ structure reacted with a relatively smaller volume of KOH ink, we employed the dip-pen nanolithography and polymer-pen lithography to react the small volume of KOH ink to a local region on the substrate. Figure 1 shows the schematic DPN process to fabricate micron $\text{Al}(\text{OH})_3$ dot patterned structures on the substrate. The DPN processes are distinguished to two methods according to the way KOH inks are transferred. At first, the liquid phase transfer is the method to transfer KOH ink to the substrate as a liquid phase (**Figure 1a**). In the liquid phase transfer process, the DPN tip is inked in the inkwell and subsequently placed to the substrate using DPN5000, dropping the micro size KOH droplets on the surface at each contact

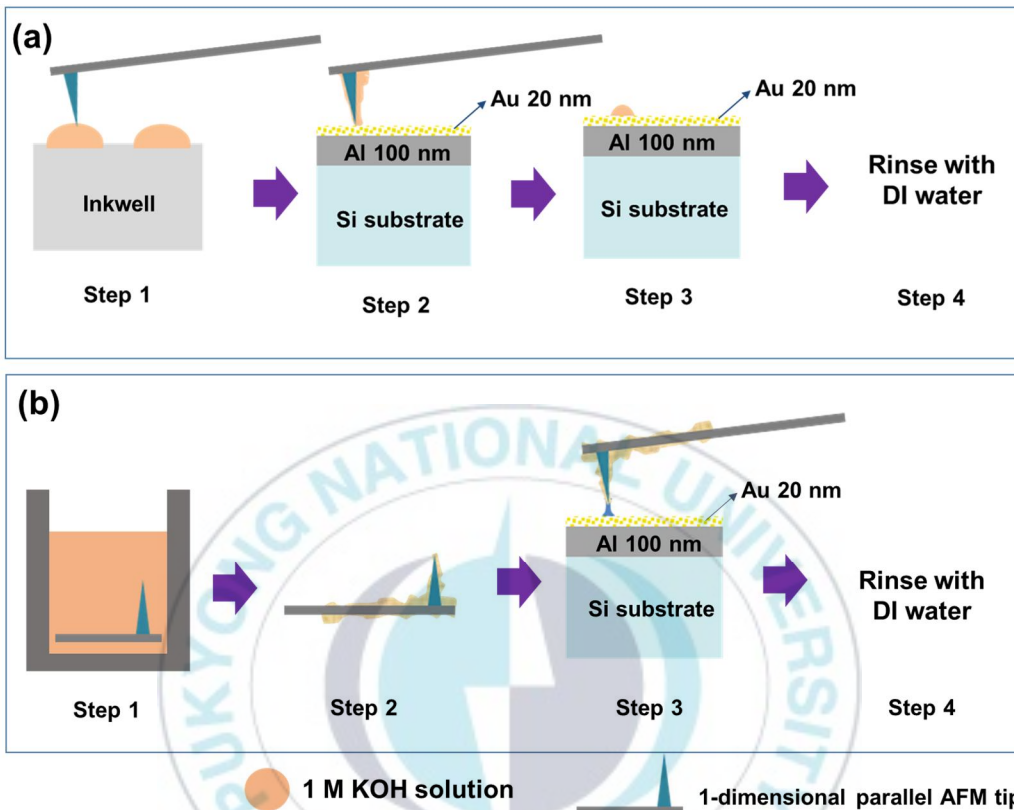


Figure 1. Schematic illustrations of the process engineering Al(OH)₃ structures on the substrate with the DPN5000. Two ink-transfer methods are illustrated. (a) liquid phase transfer, (b) solid-gel phase transfer

between the tip and the substrate. Then, the dropped KOH droplets are used to react with the Al layer under the Au membrane until the droplets are fully dried. During the reaction between the Al layer and the KOH droplet, protruded $\text{Al}(\text{OH})_3$ structures are formed on the Au membrane. Second, the solid-gel phase transfer is the method to transfer KOH ions to the substrate through a meniscus (**Figure 1b**). In the solid-gel phase transfer process, the DPN tip is immersed in 2 mL of KOH ink for 2 min, then, the tip is fully dried for 1 h under ambient atmosphere. With fully dried tip held on DPN5000, the tip is engaged to and dwells on the surface for 10 min. While the tip dwells on the surface, there formed a meniscus between the tip and the substrate which takes an important role to transfer ions to the surface. As it is formed between the tip and the substrate collecting H_2O molecules from the ambient atmosphere, the meniscus serves continuous moisture in its states acting as a local chemical reaction site. With the continuous chemical reaction, the relatively fine $\text{Al}(\text{OH})_3$ dot structures are formed on the substrate.

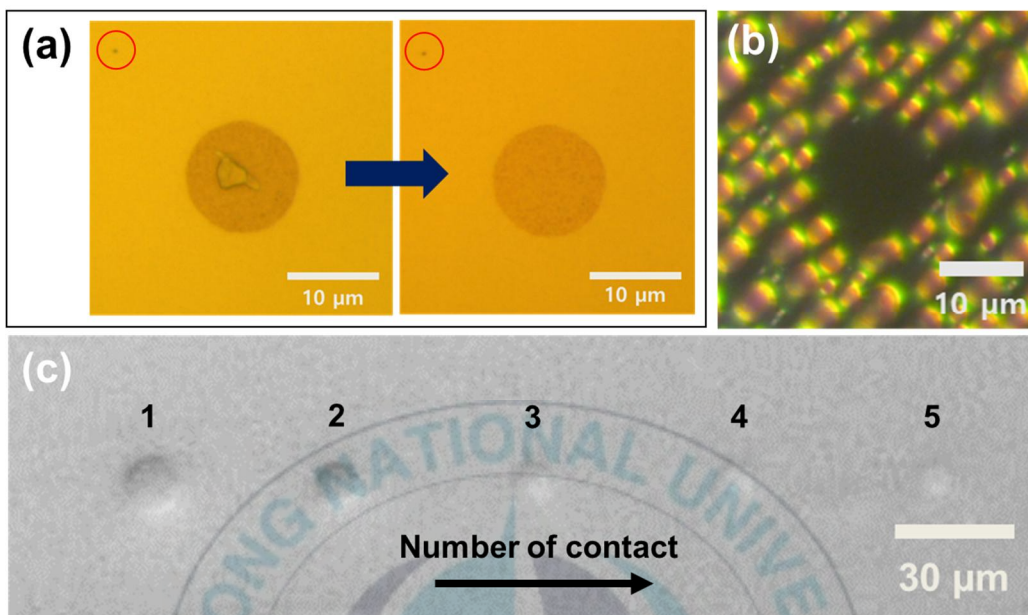
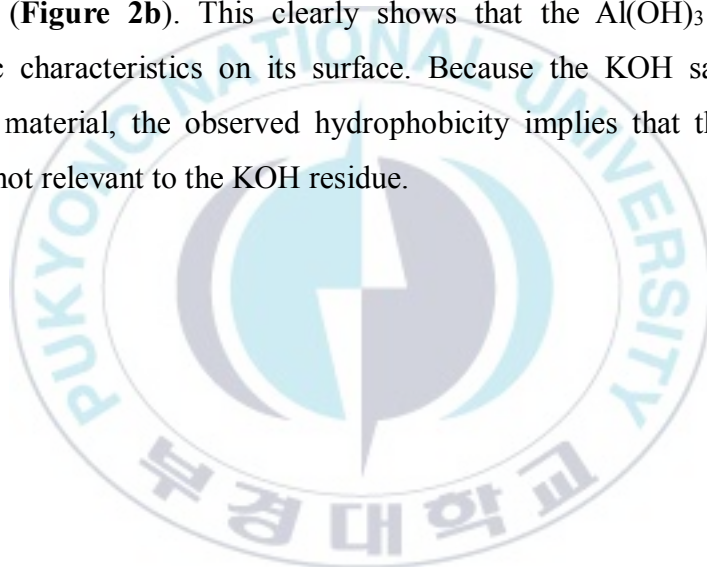


Figure 2. (a,b) Optical microscopy images of the DPN processed structure with liquid phase transfer (a) before and after the cleaning process in the bright-field image and (b) exposed to humidity in dark field image. The red circle in Figure 2a denotes the reference for the location. (c) SEM image of the DPN processed structure with liquid phase transfer depending on the number of contact between the tip and the substrate.

As shown in **Figure 2a(left)**, the irregular shaped KOH salt residue was present on the $\text{Al}(\text{OH})_3$ dot structure before a cleaning process. To eliminate the KOH salt residue, the DPN processed structures were rinsed with the flow of deionized water for 30 s and sequentially blew with N_2 gas. After the cleaning process, the residue on the $\text{Al}(\text{OH})_3$ structure disappeared, showing the engineered $\text{Al}(\text{OH})_3$ structure is insoluble in the deionized water (**Figure 2a(right)**). The resulted $\text{Al}(\text{OH})_3$ structure was exposed to water vapor during the dark-field observation using optical microscopy (**Figure 2b**). This clearly shows that the $\text{Al}(\text{OH})_3$ structure has hydrophobic characteristics on its surface. Because the KOH salt is a strong hydrophilic material, the observed hydrophobicity implies that the constructed structure is not relevant to the KOH residue.



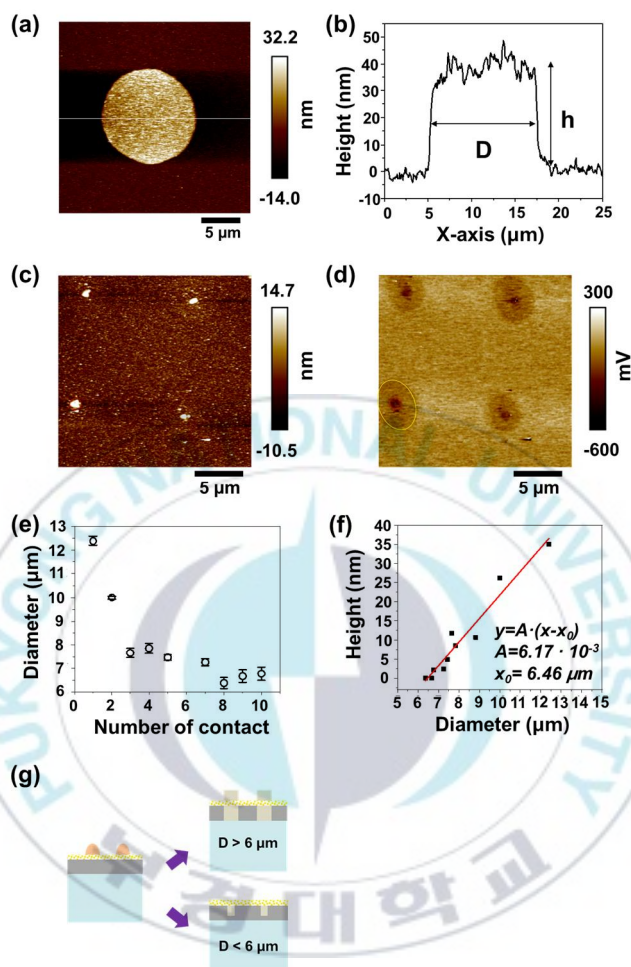


Figure 3. (a) AFM topography image of the DPN processed $\text{Al}(\text{OH})_3$ structure with liquid phase transfer and (b) the line profile of the white line in the AFM topography. (c) AFM topography and (d) electric potential mapping of the DPN processed KOH residue with liquid phase transfer. (e) Diameter dependent on the number of contact between the tip and the substrate and (f) height dependent on the diameter of the DPN processed $\text{Al}(\text{OH})_3$ structure with liquid phase transfer. (g) Schematic representation of the DPN processed $\text{Al}(\text{OH})_3$ structure depending on the diameter after the cleaning process.

As mentioned above, the DPN process through liquid phase transfer leaves KOH droplets to the substrate at each contact between the tip and the substrate. It is reported that the volume of transferred liquid droplets on a substrate has a tendency to decrease until it reaches an arbitrary equilibrium state.²⁴ The reported tendency agrees well with the decreasing in the diameter of $\text{Al}(\text{OH})_3$ structures depending on the number of contact between the tip and the substrate as shown in **Figure 2c**. To investigate the adequate tendency in structural dimension, topographic images of $\text{Al}(\text{OH})_3$ structure were measured using atomic force microscopy (AFM). The diameter of the $\text{Al}(\text{OH})_3$ dot structure is determined by measuring the horizontal length at the half of the height, while the height is determined as a difference from averaged bottom height to the averaged top height of the structure (**Figure 3b**). In **Figure 3a**, the topography of the $\text{Al}(\text{OH})_3$ dot structure formed by the KOH droplet transferred from the DPN-tip at the first contact is present. The first formed $\text{Al}(\text{OH})_3$ structure is selected as a representative of protruded $\text{Al}(\text{OH})_3$ dot structure. The protruded $\text{Al}(\text{OH})_3$ dot structure has a diameter with about 12 μm and height about 35 nm. Starting at this point, the diameter of $\text{Al}(\text{OH})_3$ structure decreases exponentially depending on the number of contact between the tip and the substrate (**Figure 3e**). The height of $\text{Al}(\text{OH})_3$ structure shows a linear relation with the diameter of the structure, presenting no protruded structure under 6 μm diameter (**Figure 3f**). Hence, we can say, at first, it is impossible to fabricate $\text{Al}(\text{OH})_3$ structure with a diameter smaller than 6 μm by liquid phase transfer. This is because of limited chemical reaction time between the KOH droplet and the substrate, as the KOH droplet is quickly dried before the completion of the reaction.

As it can be seen that KOH residue remains on the $\text{Al}(\text{OH})_3$ structure before the

cleaning process (**Figure 2a**), the KOH liquid ink changes its phase to the salt because the drying process is faster than the total chemical reaction process. This relative difference of the speeds between two processes is explicitly present in the case of the diameter smaller than 6 μm . In the region of the diameter of a structure below 6 μm , the topography and the electric potential mapping of the DPN processed structure were measured with KPFM before the cleaning process. As shown in **Figure 3c**, the KOH salt residues remain on the substrate with diameters in sub-micron and heights in tens of nanometer. The KOH residues on the substrate were not observed anymore in the topography after the cleaning process had been conducted. In the electric potential mapping, three different electric potential regions appear as indicated by a red circle line, a yellow ellipsoid line, and remained area (**Figure 3d**). The red region represents the electric potential of the KOH salt and the remained area represent the substrate while the yellow regions appear with no related topographic structures. For the electric potential of ionic crystals on a metal substrate, Reenen *et al.* reported that ionic crystal and insulator deposited on a metal substrate trigger the modification of the work function of the metal substrate.²⁵ In the study, the work function of gold substrates was modified to decrease and increase depending on the deposited materials on the substrate. In addition, Sadeghi *et al.* reported that it is difficult to define the work function of ionic crystal or insulator because the equilibration of fermi level alignment may require a considerable length of time.²⁶ Despite the limitation in quantitatively analyzing the work function of insulating materials by KPFM measurement, KPFM measurement is still a powerful tool to distinguish different elements of materials on a surface. With this point of view, the yellow regions imply that there should be

chemically reacted regions under the gold substrate because the yellow regions are only observed in the electric potential mapping, not in the topography. The two distinguished fabrication process depending on diameter ($D > 6 \mu\text{m}$, $D < 6 \mu\text{m}$) is illustrated as a scheme in **Figure 3g**. According to the scheme of the processes, the protruded structure with a diameter bigger than $6 \mu\text{m}$ are formed with the full reaction of the local Al region to $\text{Al}(\text{OH})_3$ under the Au film and sequence protrusion of $\text{Al}(\text{OH})_3$ on the Au film. On the other hand, in the region of a diameter smaller than $6 \mu\text{m}$, only local Al region under the Au film are reacted to $\text{Al}(\text{OH})_3$ with KOH salt residue on the Au film. The difference between the two regions is due to the total reaction time during which KOH droplet act as a chemical reaction site. In the first place, the volume of the KOH droplet is enough to react local Al region under the Au film until the reaction results in protrusion before the KOH droplet dry. Still, the whole KOH droplet can't join the reaction process and eventually become KOH residue on the protruded $\text{Al}(\text{OH})_3$ structure as shown in **Figure 2a**. On the contrary, a relatively smaller volume of the KOH droplet only has time to react a part of local Al layer under Au film because it dries faster. As a result, only KOH residues are left on the Au film without protruded $\text{Al}(\text{OH})_3$ structure and the KOH residues are eliminated by the cleaning process.

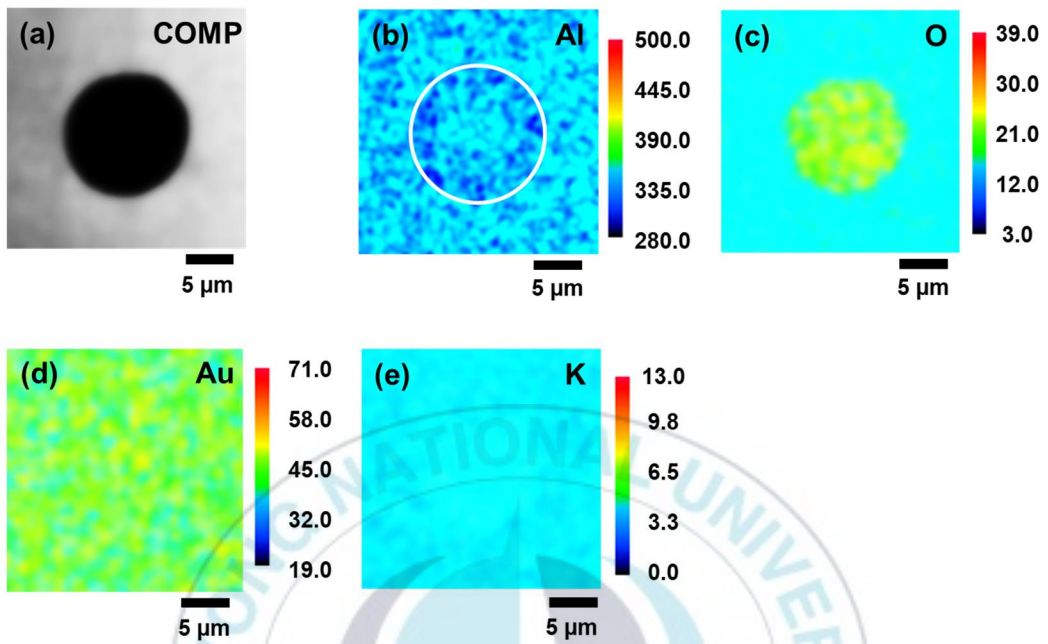


Figure 4. Electron probe micro-analysis on the DPN processed structure with liquid phase transfer. (a) BSE image and characteristic x-ray mapping image of (b) Al, (c) O, (d) Au, and (e) K.

The resulted structure after cleaning process in **Figure 3a** was investigated to analyze the elements of the structure using EPMA (**Figure 4**). In **Figure 4a**, the region of the structure is shown by the backscattered electron image. This shows that the engineered structure has much smaller atomic number than the Au film. Thus, the element in the structure is certainly distinguished from the element in the substrate. Ironically, the EPMA mapping on Al element (**Figure 4b**) shows less intensity in the structure than the substrate. This is because the density of Al in the structure is less than the Al layer under Au film. As the Al elements in the protruded region are reacted with hydroxide ions, the volume of the reacted region become bigger with the amount of Al elements being maintained. A similar study about lower EPMA intensity to oxidized Al layer than pure Al layer was reported by Dade *et al.*²⁷ By contrast, the component of hydroxide ion in the structure was identified by the EPMA mapping on oxygen element (**Figure 4c**), showing higher EPMA intensity in the dot structure. The high EPMA intensity of oxygen element in the structure with the negligible low EPMA intensity of potassium element (**Figure 4e**) shows that the dot structure is oxidized material with the bare presence of the KOH residue. Therefore, the structure is regarded as an aluminum region oxidized with hydroxide ion. In addition, the EPMA intensity in Au element was observed to be uniform on the whole area of the substrate.

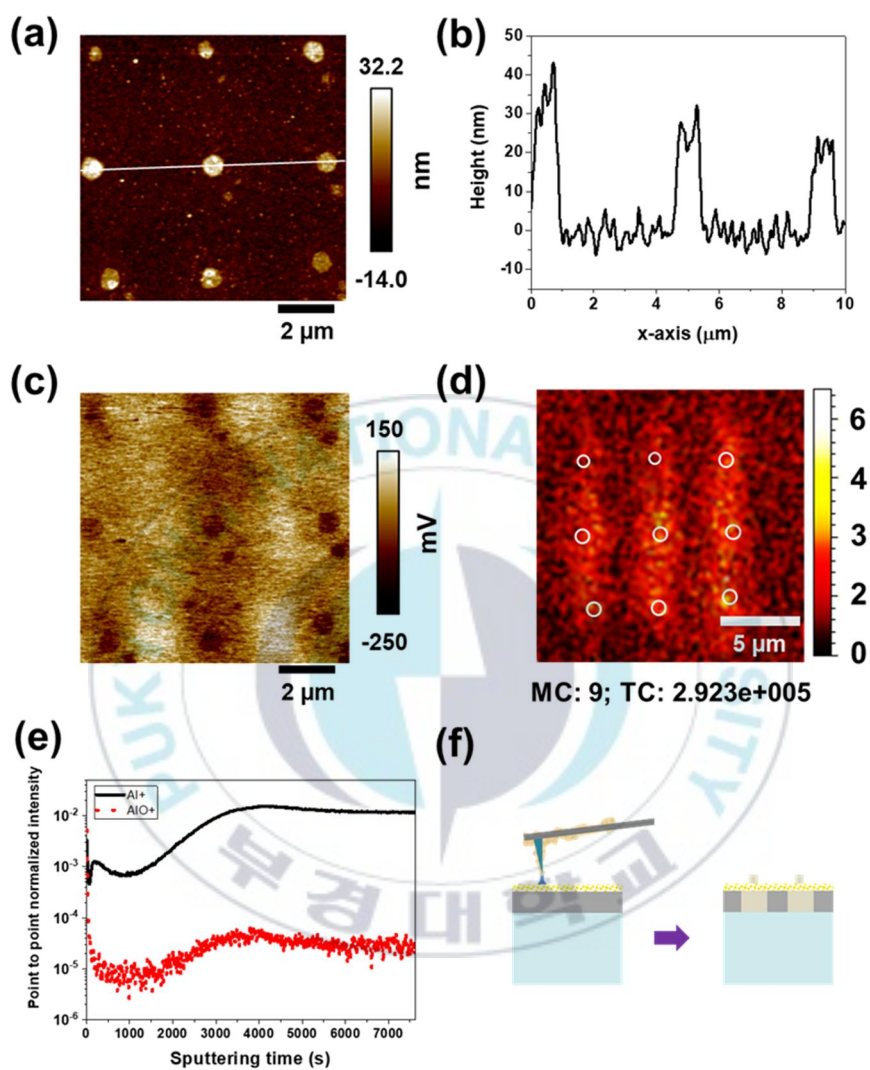


Figure 5. (a) AFM topography image of the DPN processed $\text{Al}(\text{OH})_3$ structure with solid-gel phase transfer and (b) line profile of the white line in the AFM topography. (c) Electric potential mapping and (d) TOF-SIMS image of the structure. (e) Depth profile of Al^+ and AlO^+ elements in the structure. (f) Schematic representation of the DPN processed $\text{Al}(\text{OH})_3$ structure with solid-gel phase transfer.

The DPN processed structures with the solid-gel phase transfer (**Figure 1b**) were investigated. The topographies of the DPN processed structures with the solid-gel phase transfer are shown in **Figure 5a,b**. The 3×3 patterns of the structure were engineered in a sequence from left to right in a row, and a row followed from the top to the bottom. Each dot was fabricated by dwelling the tip to the substrate for 10 min. In contrast to the DPN processed structure with liquid phase transfer, the dimension in diameter and height of the DPN processed structure with the solid-gel phase transfer show relatively consistent. This relatively uniform size in the dimension of the solid-gel phase transfer is possible because we can decide the chemical reaction time by controlling the dwelling time of the tip to the substrate. However, it is assumed that a stabilization process is required for uniform fabrication of the structure, as the first and second fabricated dot structure in **Figure 5a** is relatively smaller than the dots fabricated later. This is because, in the drying process, the KOH salts are dried on the cantilever with irregular shape and relative location to the tip. Hence, at first and second fabrication, the OH^- ion transfer to the substrate via the meniscus is unstable. Once the ion transfer rate is stabilized, it is easily obtained to fabricate structures with consistent diameter and height. In **Figure 6a**, the consistent dimension in diameter is saturated to $1 \mu\text{m}$ with dwell-time longer than 10 min. When it takes 1 min to dwell the tip to the substrate after the stabilization, the averaged diameter and height of the structure is about 300 nm, 15 nm, respectively. The tendency for the dimension to saturate to some extent means that the lithographic process has an upper limitation in its diameter and height. The limitation comes from the role of the meniscus to fabricate the structure. Because the meniscus takes a role as a chemical reaction site, the size of the

meniscus decides the upper limitation of the structure. In other words, the magnitude of the engineered structure can not exceed the size of the meniscus. The reacted regions in DPN processed structure with solid-gel phase transfer were detected in an electric potential mapping. Similar to the reacted regions of the DPN processed sample with liquid phase transfer, the reacted regions under Au film also present in the sample with the solid-gel phase transfer as three lines in a direction of a column (**Figure 5c**). The reacted regions under Au film do not appear in the topography. Furthermore, the sample was investigated for element analysis using a TOF-SIMS measurement. As shown in **Figure 5d**, the reacted regions were characterized as aluminum complex. By comparison, the shape of the reacted regions detected by the electric potential agree well with the shape of the aluminum reacted region. In order to confirm the structure is aluminum complex, depth profiles for Al^+ , AlO^+ were investigated (**Figure 5e**). Thomas Stephan reported AlO^+ signal is attained from the monoisotopic aluminum element by TOF-SIMS analysis.²⁸ However, AlO^+ signal from aluminum (hydr)oxide materials has not been reported yet. Therefore, both Al^+ and AlO^+ signals are detected from Al layer under Au film while only Al^+ signal can be detected from aluminum (hydr)oxide structure. For this reason, the exceptional parabolic peak presenting in Al^+ signal is proof of the existence of the Aluminum (hydr)oxide structure.

In the region of diameter smaller than 6 μm , the topography and phase image of the DPN processed structure with solid-gel transfer and the KOH residue with liquid phase transfer were attained using AFM measurement. Here, the structures made by solid-gel transfer did not vanish after the cleaning process, while the KOH residues by liquid phase transfer were easily removed. Besides, the phase between

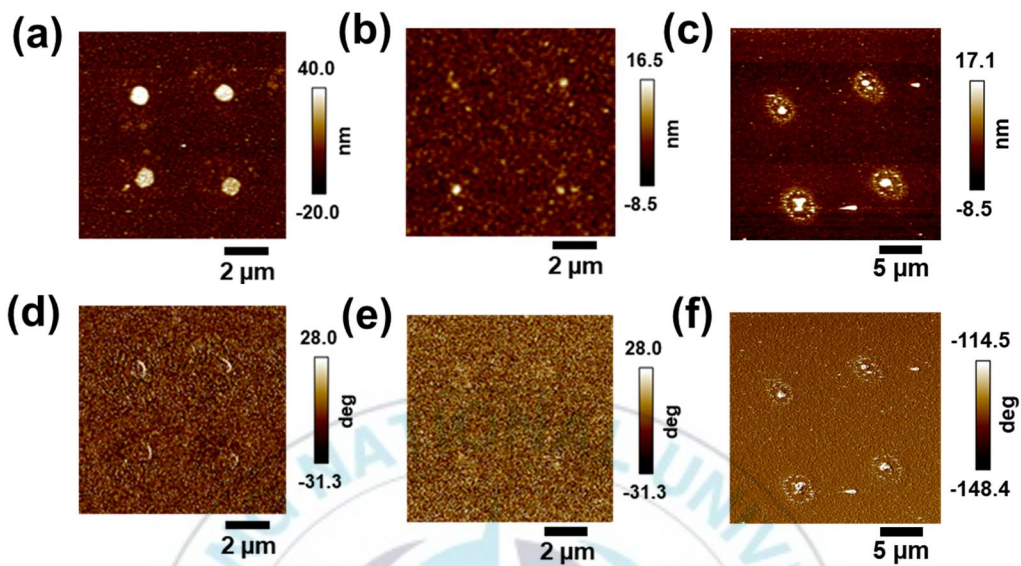


Figure 6. AFM topography and phase image of the DPN processed $\text{Al}(\text{OH})_3$ structure with solid-gel phase transfer: (a,d) dwell time for 10 min, (b,e) 1 min, and (c,f) of the DPN processed KOH residue with the liquid phase transfer.

the sample and the substrate shows difference depending on the transfer method. The phase of the structure made by solid-gel phase transfer is similar to the phase of the Au film, whereas the phase of KOH residue on the substrate has a distinguishable difference to the phase of Au film. As a result, aluminum hydroxide structures with a diameter smaller than 6 μm can be obtained only by the solid-gel phase transfer.



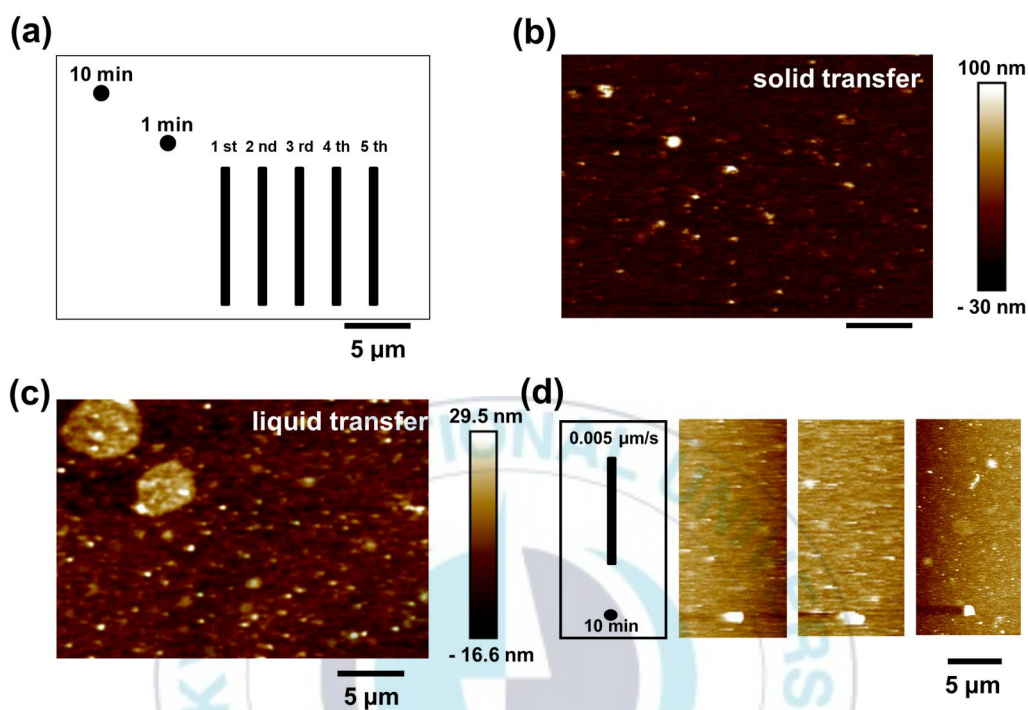


Figure 7. (a) Schematic illustration for the DPN processed dot and line pattern. (b) AFM topography image of the DPN processed pattern by solid-gel phase transfer and (c) liquid phase transfer. (d) Schematic illustration and AFM topography of the DPN processed pattern with lowest line scan speed (0.005 μm/s) by solid-gel phase transfer method.

In order to investigate the possibility of engineering line structure, the DPNs are carried out with the solid-gel phase transfer and liquid phase transfer, respectively (**Figure 7**). **Figure 7a** shows the scheme of the sequence to fabricate dot and line patterns. At first, a dot structure was engineered with dwelling the tip to the substrate for 10 min. Sequence, a dot structure with dwell-time 1 min was engineered. The sequenced fabrication of two dots was for the stabilization of the tip to transfer and the identification of relative location between structures. Then, the engineering processes for the line structures were conducted from up to down. The scan speed of the tip employed to engineer the line structures were 0.005 $\mu\text{m/s}$, 0.01 $\mu\text{m/s}$, 0.05 $\mu\text{m/s}$, 0.1 $\mu\text{m/s}$, and 0.5 $\mu\text{m/s}$ for a sequence from 1st to 5th line. The lowest scan speed for 0.005 $\mu\text{m/s}$ was decided as it is the lowest limitation we can employ via the DPN software. In solid-gel phase transfer, two dot structures were engineered at each location with the first dot structure unsaturated due to the stabilization process. However, the line structures were not engineered. The absence of the line structure even at lowest scan speed (0.005 $\mu\text{m/s}$) is considered to result from the instability of meniscus as a chemical reaction site, because the meniscus is constantly influenced by the mechanical movement of the tip.

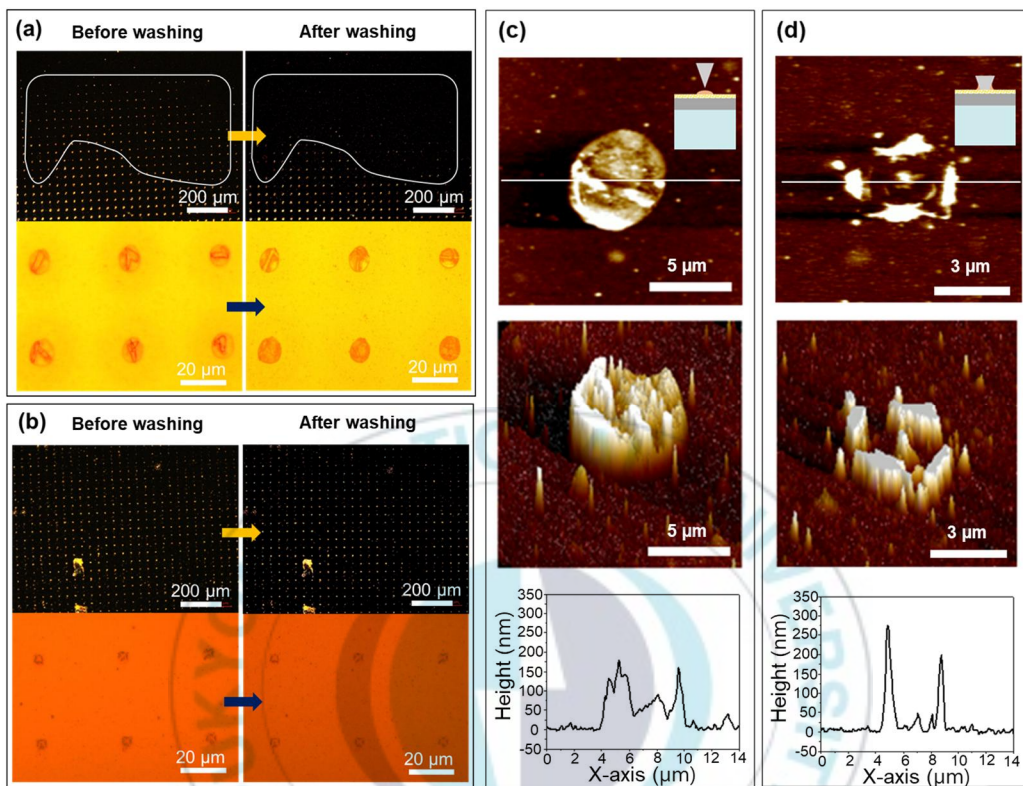


Figure 8. Optical microscopy image of PPL processed structure with (a) liquid phase transfer and (b) solid-gel phase transfer: upper dark-field images present large patterned structure before and after the cleaning process and below bright-field images present same structure with magnified resolution. 2D, 3D AFM topography images and line profile of the white line in the PPL processed structure with (c) liquid phase transfer and (d) solid-gel phase transfer

Briefly so far, it is possible to fabricate sub-micron, micron metal oxide dot structure by local chemical reaction of the substrate using the DPN. Based on the concept of a local chemical reaction using tips, we can introduce PPL for large-area fabrication. The optical microscopic image for large area fabricated $\text{Al}(\text{OH})_3$ patterned structure and topography for the individual structure were displayed for the liquid phase transfer method (**Figure 8a,c**) and the solid-gel phase transfer (**Figure 8b,d**), respectively. The PPL processed structure with liquid phase transfer shows similar trends for the fabrication process with the DPN processed structure with liquid phase transfer. In the region of diameter bigger than $4\ \mu\text{m}$, protruded dot structures were formed with KOH residue on the dot structure. The KOH residues on the structure were easily removed after a cleaning process rinsing with deionized water as indicated by blue arrow in **Figure 8a**. In the cleaning process, structures with a diameter smaller than $4\ \mu\text{m}$ (white envelope in **Figure 8a**) disappear, implying structures with a diameter smaller than $4\ \mu\text{m}$ were just KOH residue. The lower limit of the diameter $4\ \mu\text{m}$ in the structure made by PPL with liquid phase transfer is lower than the lower limit of the diameter $6\ \mu\text{m}$ in the structure made by DPN with liquid phase transfer. The difference in the lower limit of the diameter comes from the difference between local humidity between the two processes. When the liquid phase transfer is employed by PPL, PPL introduces large-area patterned KOH droplets on the substrate. Because of the plenty number of KOH droplets on the substrate, the Al layer under the Au film reacts not locally with individual KOH droplet, but entirely with the group of the KOH droplets. It makes easier environments to form protruded $\text{Al}(\text{OH})_3$ structure, resulting in the lower limit of the diameter of the structure. In contrast, the structures made by PPL

with solid-gel phase transfer were not eliminated after the cleaning process. In fact, the KOH residues were not observed on the structure before the cleaning process. As the meniscus acted as a chemical reaction site during the whole process, the KOH salt could not remain on the structure. As a consequence, sub-micron wall structures could be formed using PPL with solid-gel phase transfer. Furthermore, the wall shaped structure is the proof for the meniscus acts as a chemical reaction site. In general, the conventional micro-contact method with PPL was reported that the target ink is transferred with the shape of “x”.²⁹ However, the wall shaped structure obtained in this study is the exactly reciprocal shape of the conventional PPL micro-contact processed structure. This means that the structures in this study were made in the meniscus formed between the side of the polymer pen and the substrate as shown in the inset of **Figure 8d**. If they are not engineered via the chemical reaction within the meniscus, the structure should be formed on the substrate where the tip is in contact. The constructed structure consists of 4 walls at each side with a width about 300 nm and a height about 200 nm. The distance between the walls is about 4 μm . Because the walls are located at the four cardinal points, the structures have the potential to be employed as a cavity to two directions.

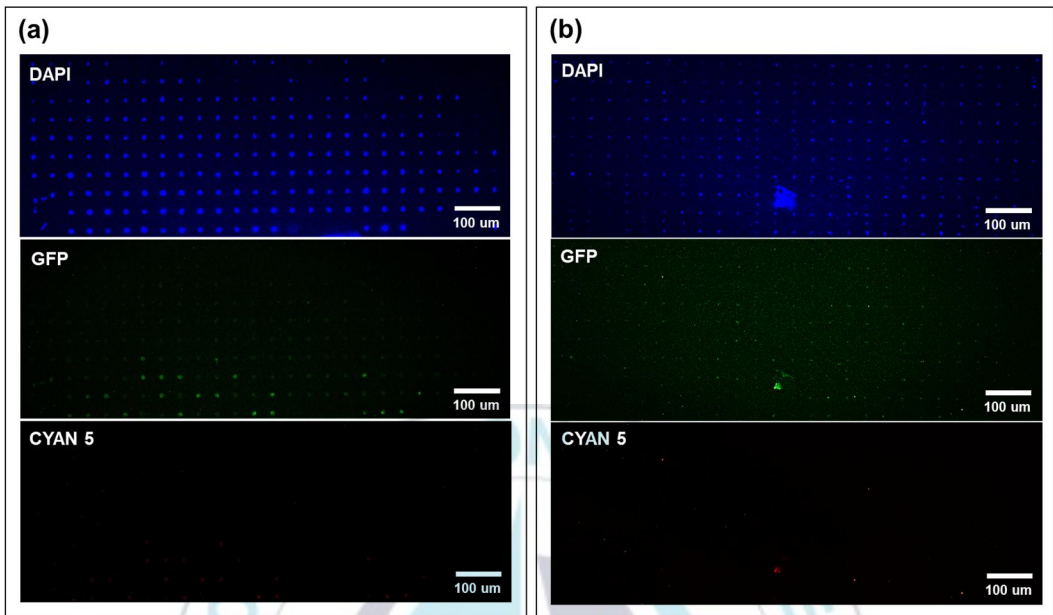
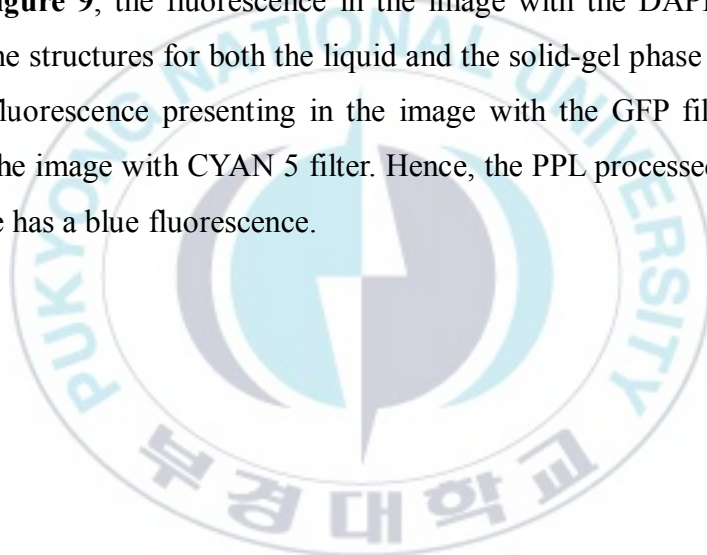


Figure 9. Fluorescence images of the PPL processed structure with (a) liquid phase transfer and (b) solid-gel phase transfer: excitation wavelength (λ_{ex}) of 365 nm and emission wavelength (λ_{em}) of 445 nm in DAPI filter, λ_{ex} of 475 nm and λ_{em} of 530 nm in GFP filter, λ_{ex} of 545 nm and λ_{em} of 605 nm in CYAN 5 filter

The fluorescence images of the PPL processed samples with liquid and solid-gel phase transfers were characterized at three pairs of fluorescence filters with different wavelengths for excitation and emission, respectively (**Figure 9**). To be specific, the DAPI filter was used to filter the wavelength of the Hg lamp to 365 nm and 445 nm as an excitation wavelength (λ_{ex}), emission wavelength (λ_{em}), respectively. In addition, the excitation and emission wavelength is 475 nm and 530 nm for the GFP filter, while 545 nm and 605 nm for the CYAN 5 filter. As shown in **Figure 9**, the fluorescence in the image with the DAPI filter is most explicit in the structures for both the liquid and the solid-gel phase transfers, with a little bit fluorescence presenting in the image with the GFP filter and barely existing in the image with CYAN 5 filter. Hence, the PPL processed structures on the substrate has a blue fluorescence.



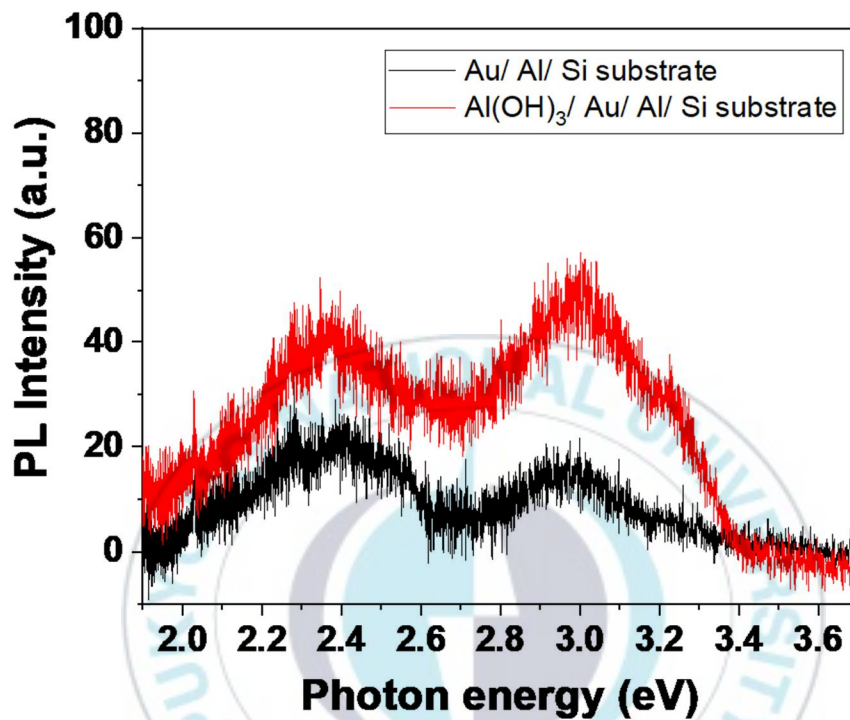


Figure 10. The micro photoluminescence emission spectrum of the PPL processed Al(OH)₃ structure (black) and the substrate (red) excited by the laser with wavelength at 325 nm (3.81 eV)

In order to investigate the origin of the blue fluorescence, we obtained the photoluminescence spectrum of the PPL processed structure by solid-gel phase transfer on the substrate using an excitation laser at 325 nm. **Figure 10** shows the photoluminescence spectrum of the PPL structure (black) and the substrate (red). At first, the largest photoluminescence peak at 1.6 eV was reported as photoluminescence from Si clusters.³⁰ As it is indicated later, the photoluminescence at 1.6 eV was not observed on the substrate with a glass substrate as an alternative of Si substrate (**Figure 11b,c**). In addition to the photoluminescence peak of the silicon substrate, two peaks were observed at 2.36 eV and 3.0 eV on the substrate. Specifically, G. T. Boyd *et al.* reported the two peaks at 2.36 eV and 3.0 eV in the photoluminescence exactly originated from a gold film with a rough surface with excitation wavelength at 3.50 eV (354 nm).³¹ In the study, the photoluminescence at 2.36 eV is derived from the transition of excited electrons in the 6 sp band to the 5 d band near the L symmetry point (6 – 5 L transitions), while the photoluminescence at 3.0 eV is due to the 6 – 4 L transitions. With the result, the intensity of photoluminescence in the Al(OH)₃ structure was found to enhance the transitions of excited electrons in the Au film in the whole region of the spectrum. Especially, the 6 – 5 L transitions were enhanced relatively bigger than the 6 – 4 L transitions. The relative enhancement in the transitions is compatible with the relative intensity of the fluorescence as shown in **Figure 9**.

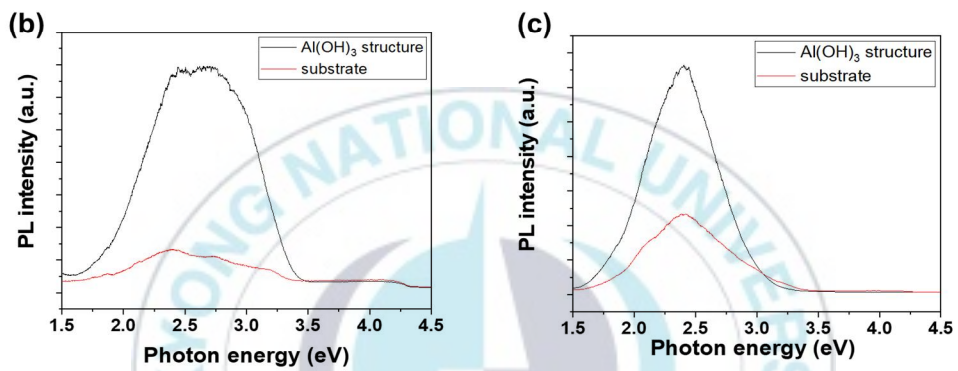
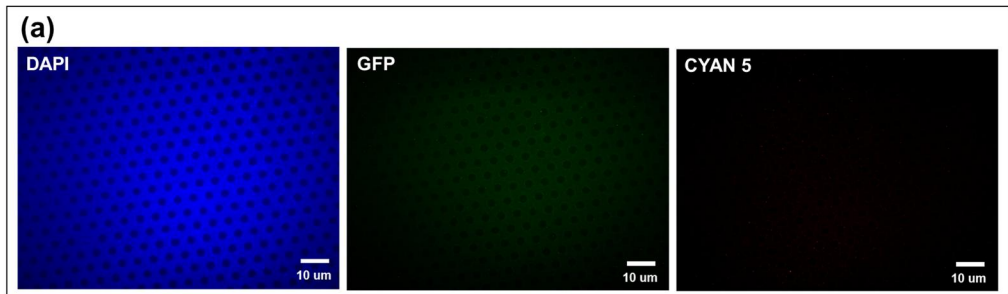


Figure 11. (a) Fluorescence image of the macro hole $\text{Al}(\text{OH})_3$ structure in a sequence of the DAPI filter (left), the GFP filter (center), the CYAN 5 filter (right). The macro photoluminescence emission spectrum of the macro hole $\text{Al}(\text{OH})_3$ structure (black) and the substrate (red) excited by the laser with wavelength at (b) 325 nm (3.81 eV) and (c) 266 nm (4.66 eV).

To confirm the photoluminescence characteristic in $\text{Al}(\text{OH})_3$ structure, we introduced the macro hole $\text{Al}(\text{OH})_3$ structure by molding 1M KOH ink to the 30 nm Au film on the 200 nm Al deposited glass substrate, followed by the fabrication process in our previous study.²²⁻²³ As shown in **Figure 11a**, the macro hole $\text{Al}(\text{OH})_3$ structure has an analogous fluorescence characteristic with the PPL processed $\text{Al}(\text{OH})_3$ structure, presenting the highest intensity of fluorescence with the DAPI filter. For the macro photoluminescence measurement, the excitation laser with wavelength at 325 nm was employed as the equivalent excitation source in the micro photoluminescence (**Figure 11b**). The measured photoluminescence spectrum in the macro hole $\text{Al}(\text{OH})_3$ structures presents a broad peak ranged from 1.8 eV to 3.3 eV which is analogous to the PPL processed $\text{Al}(\text{OH})_3$ structure. In addition, the intensity of photoluminescence in the region with the energy level bigger than 2.5 eV was enhanced more than in the region with the energy level smaller than 2.4 eV, which is corresponding trends to the photoluminescence in the PPL processed structure. Hence, we regard the broad photoluminescence peak of macro hole $\text{Al}(\text{OH})_3$ structure as the summation of two peaks from 2.34 eV (6 – 5 L transitions) and 3.0 eV (6 – 4 L transitions), as well. Additionally, the photoluminescence spectrum of the macro hole $\text{Al}(\text{OH})_3$ structure was measured using a 266 nm wavelength diode-pumped solid-state laser as an excitation source (**Figure 11c**). Abnormally, the photoluminescence spectrum excited by 266 nm wavelength laser source shows narrower emission peak than the photoluminescence spectrum by 325 nm wavelength, whereas it is usually expected that a laser source with higher energy produces more excited energy states. The untypical trend in the photoluminescence spectrum was also identified as

photoluminescence of a gold film with rough surface excited by 4.67 eV (265 nm) laser source, generating 6 – 5 L transitions and 6 – 4 X transitions.³¹



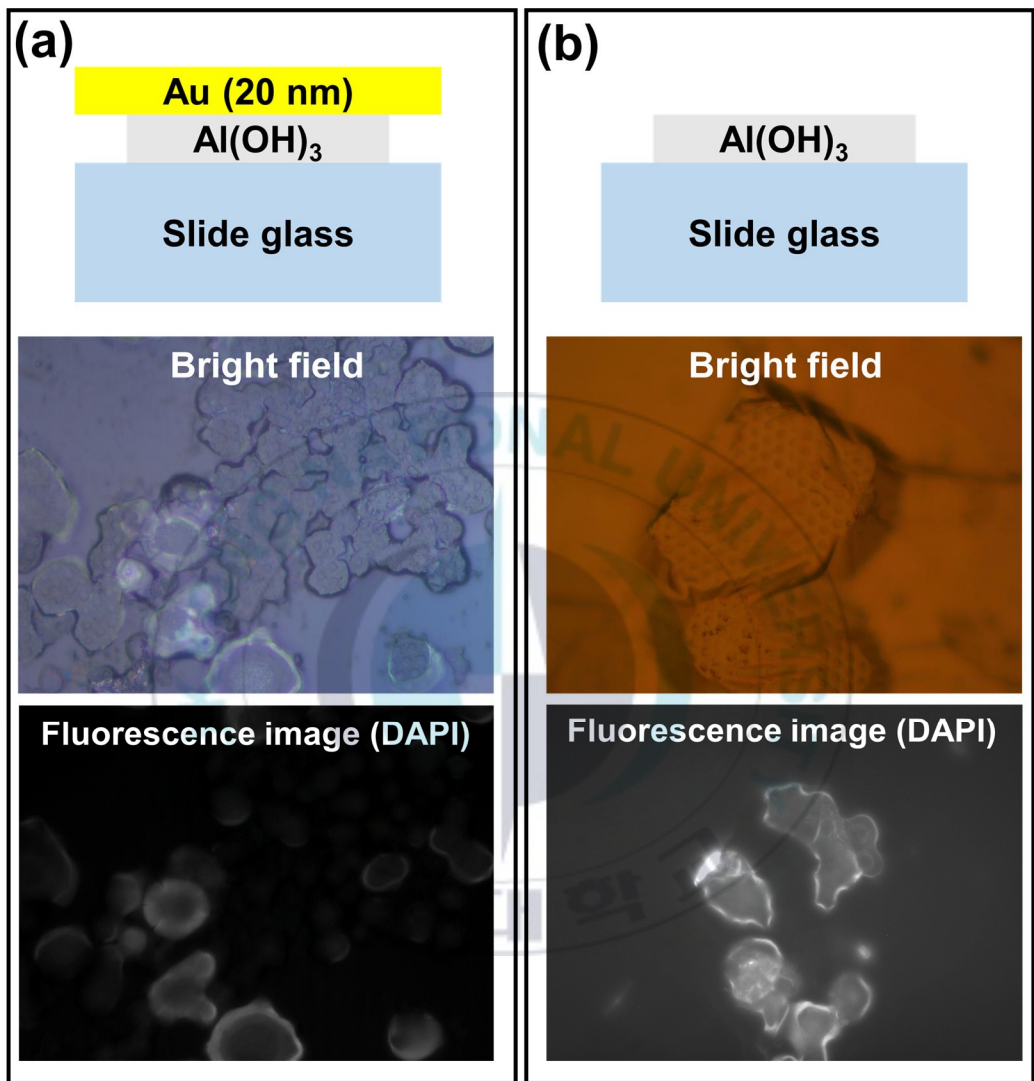
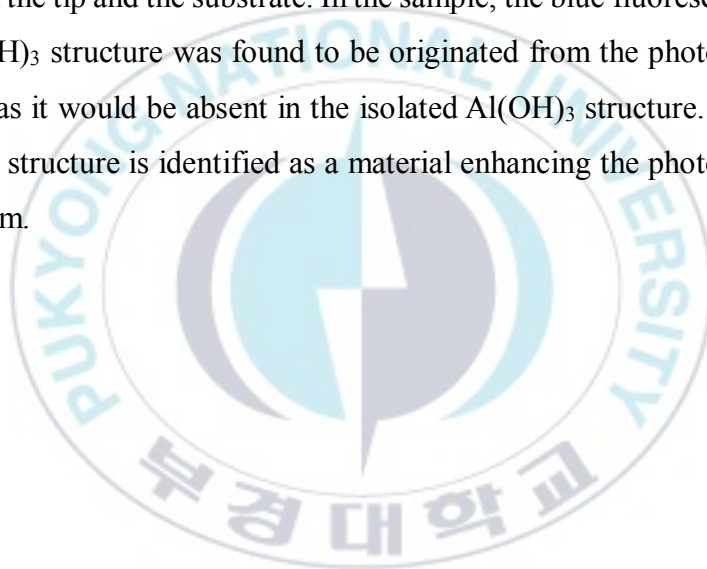


Figure 12. Schematic illustration, optical microscopy in bright field and fluorescence image in the DAPI filter of (a) the transferred Au/ macro hole Al(OH)₃ structure/ glass substrate and (b) macro hole Al(OH)₃ structure/ glass substrate after etching Au film.

To prove our analysis, the macro hole $\text{Al}(\text{OH})_3$ structure on the substrate was immersed in 1M KOH solution to etch Al layer and separate the macro hole $\text{Al}(\text{OH})_3$ on Au film from the substrate. As a sequence, the separated macro hole $\text{Al}(\text{OH})_3$ on Au film was transferred in the opposite direction to the slide glass as shown in the scheme in **Figure 12a**. Even in the opposite direction, the reverse structure of macro hole $\text{Al}(\text{OH})_3$ and Au film still showed fluorescence, however, the hole shape of the structure was not clear in the fluorescence. It is considered that the Au film on the $\text{Al}(\text{OH})_3$ structure disturb the emission of the fluorescence. Finally, the Au film on the $\text{Al}(\text{OH})_3$ structure was etched by aqua regia solution. The fluorescence of the isolated macro hole $\text{Al}(\text{OH})_3$ structure on the glass did not occur anymore. Hence, the blue fluorescence in the PPL processed structure was proved to be originated from the photoluminescence in the Au film. However, the metal photoluminescence has extraordinary low photoluminescence quantum yield ($\sim 10^{-10}$), the presence of $\text{Al}(\text{OH})_3$ structure is essential to enhance the photoluminescence of the gold film. In addition, the mechanism of the metal photoluminescence enhancement by $\text{Al}(\text{OH})_3$ is obscure, it is highly required to understand the enhancement process for the future study.

Conclusion

The $\text{Al}(\text{OH})_3$ structure was fabricated on the Au/ Al/ Si substrate using the DPN and PPL. In each lithographic techniques, OH^- ions were transferred to the substrate and react with the Al layer under the Au film by the liquid phase transfer and solid-gel phase transfer. In solid-gel phase transfer, it is possible to fabricate sub-micron $\text{Al}(\text{OH})_3$ structure as the meniscus is formed continuously as a chemical reaction site between the tip and the substrate. In the sample, the blue fluorescence observed on the $\text{Al}(\text{OH})_3$ structure was found to be originated from the photoluminescence of Au film, as it would be absent in the isolated $\text{Al}(\text{OH})_3$ structure. Consequently, the $\text{Al}(\text{OH})_3$ structure is identified as a material enhancing the photoluminescence of the Au film.



Reference

1. Hu, H. K., H.J.; Somnath, S., Tip-Based Nanofabrication for Scalable Manufacturing. *Micromachines* **2017**, *8*, 90.
2. Eigler, D. M.; Schweizer, E. K., Positioning Single Atoms with a Scanning Tunnelling Microscope. *Nature* **1990**, *344*, 524.
3. Shen, T. C.; Wang, C.; Abeln, G. C.; Tucker, J. R.; Lyding, J. W.; Avouris, P.; Walkup, R. E., Atomic-Scale Desorption through Electronic and Vibrational Excitation Mechanisms. *Science* **1995**, *268*, 1590.
4. Dai, Z.; King, W. P.; Park, K., A 100 Nanometer Scale Resistive Heater–Thermometer on a Silicon Cantilever. *Nanotechnology* **2009**, *20*, 095301.
5. Garcia, R.; Martinez, R. V.; Martinez, J., Nano-Chemistry and Scanning Probe Nanolithographies. *Chemical Society Reviews* **2006**, *35*, 29.
6. Day, H. C.; Allee, D. R., Selective Area Oxidation of Silicon with a Scanning Force Microscope. *Applied Physics Letters* **1993**, *62*, 2691.
7. Smolyaninov, I. I.; Mazzoni, D. L.; Davis, C. C., Near Field Direct Write Ultraviolet Lithography and Shear Force Microscopic Studies of the Lithographic Process. *Applied Physics Letters* **1995**, *67*, 3859.
8. Jersch, J.; Dickmann, K., Nanostructure Fabrication Using Laser Field Enhancement in the Near Field of a Scanning Tunneling Microscope Tip. *Applied Physics Letters* **1996**, *68*, 868.
9. Piner, R. D.; Zhu, J.; Xu, F.; Hong, S.; Mirkin, C. A., "Dip-Pen" Nanolithography. *Science* **1999**, *283*, 661.
10. Sheehan, P. E.; Whitman, L. J., Thiol Diffusion and the Role of Humidity in "Dip Pen Nanolithography". *Physical Review Letters* **2002**, *88*, 156104.

11. Weeks, B. L.; Noy, A.; Miller, A. E.; De Yoreo, J. J., Effect of Dissolution Kinetics on Feature Size in Dip-Pen Nanolithography. *Physical Review Letters* **2002**, *88*, 255505.
12. Salaita, K.; Wang, Y.; Mirkin, C. A., Applications of Dip-Pen Nanolithography. *Nature Nanotechnology* **2007**, *2*, 145.
13. Jiang, X.; Wu, G.; Du, Z.; Ma, K.-J.; Shirakashi, J.-i.; Tseng, A. A., Nanoscale Scratching of Platinum Thin Films Using Atomic Force Microscopy with DLC Tips. *Journal of Vacuum Science & Technology B* **2012**, *30*, 021605.
14. Dobisz, E. A.; Marrian, C. R. K.; Salvino, R. E.; Ancona, M. A.; Perkins, F. K.; Turner, N. H., Reduction and Elimination of Proximity Effects. *Journal of Vacuum Science & Technology B: Microelectronics and Nanometer Structures Processing, Measurement, and Phenomena* **1993**, *11*, 2733.
15. Dagata, J. A.; Schneir, J.; Harary, H. H.; Evans, C. J.; Postek, M. T.; Bennett, J., Modification of Hydrogen Passivated Silicon by a Scanning Tunneling Microscope Operating in Air. *Applied Physics Letters* **1990**, *56*, 2001.
16. Jang, J.-W.; Sanedrin, R. G.; Maspoeh, D.; Hwang, S.; Fujigaya, T.; Jeon, Y.-M.; Vega, R. A.; Chen, X.; Mirkin, C. A., Electrically Biased Nanolithography with KOH-Coated AFM Tips. *Nano Letters* **2008**, *8*, 1451.
17. Li, Y.; Maynor, B. W.; Liu, J., Electrochemical AFM “Dip-Pen” Nanolithography. *Journal of the American Chemical Society* **2001**, *123*, 2105.
18. Huo, F.; Zheng, Z.; Zheng, G.; Giam, L. R.; Zhang, H.; Mirkin, C. A., Polymer Pen Lithography. *Science* **2008**, *321*, 1658.
19. Urtizbera, A.; Hirtz, M.; Fuchs, H., Ink Transport Modelling in Dip-Pen Nanolithography and Polymer Pen Lithography. *Nanofabrication* **2016**, *2*, 43.

20. Biswas, S.; Brinkmann, F.; Hirtz, M.; Fuchs, H., Patterning of Quantum Dots by Dip-Pen and Polymer Pen Nanolithography. *Nanofabrication* **2015**, *2*, 19.
21. O'Connell, C. D.; Higgins, M. J.; Marusic, D.; Moulton, S. E.; Wallace, G. G., Liquid Ink Deposition from an Atomic Force Microscope Tip: Deposition Monitoring and Control of Feature Size. *Langmuir* **2014**, *30*, 2712.
22. Oh, C.-M.; Park, K. H.; Choi, J.-H.; Hwang, S.; Noh, H.; Yu, Y. M.; Jang, J.-W., Polycrystalline Au Nanomembrane as a Tool for Two-Tone Micro/Nanolithography. *Chemistry of Materials* **2017**, *29*, 3863.
23. Choi, J.-H.; Oh, C.-M.; Jang, J.-W., Micro- and Nano-Patterns Fabricated by Embossed Microscale Stamp with Trenched Edges. *RSC Advances* **2017**, *7*, 32058.
24. O'Connell, C. D.; Higgins, M. J.; Sullivan, R. P.; Moulton, S. E.; Wallace, G. G., Ink-on-Probe Hydrodynamics in Atomic Force Microscope Deposition of Liquid Inks. *Small* **2014**, *10*, 3717.
25. van Reenen, S.; Kouijzer, S.; Janssen, R. A. J.; Wienk, M. M.; Kemerink, M., Origin of Work Function Modification by Ionic and Amine-Based Interface Layers. *Advanced Materials Interfaces* **2014**, *1*, 1400189.
26. Sadeghi, A.; Baratoff, A.; Ghasemi, S. A.; Goedecker, S.; Glatzel, T.; Kawai, S.; Meyer, E., Multiscale Approach for Simulations of Kelvin Probe Force Microscopy with Atomic Resolution. *Physical Review B* **2012**, *86*, 075407.
27. Dadé, M.; Esin, V. A.; Nazé, L.; Sallot, P., Short- and Long-Term Oxidation Behaviour of an Advanced Ti₂AlNb Alloy. *Corrosion Science* **2019**, *148*, 379.
28. Stephan, T., TOF-SIMS in Cosmochemistry. *Planetary and Space Science* **2001**, *49*, 859.

29. Brinkmann, F.; Hirtz, M.; Greiner, A. M.; Weschenfelder, M.; Waterkotte, B.; Bastmeyer, M.; Fuchs, H., Interdigitated Multicolored Bioink Micropatterns by Multiplexed Polymer Pen Lithography. *Small* **2013**, *9*, 3266.
30. Sias, U. S.; Moreira, E. C.; Ribeiro, E.; Boudinov, H.; Amaral, L.; Behar, M., Photoluminescence from Si Nanocrystals Induced by High-Temperature Implantation in SiO₂. *Journal of Applied Physics* **2004**, *95*, 5053.
31. Boyd, G. T.; Yu, Z. H.; Shen, Y. R., Photoinduced Luminescence from the Noble Metals and Its Enhancement on Roughened Surfaces. *Physical Review B* **1986**, *33*, 7923.

